JACS
JOURNAL OF THE AMERICAN CHEMICAL SOCIETY
Article
pubs.acs.org/JACS

A Highly Sensitive Mixed Lanthanide Metal–Organic Framework Self-Calibrated Luminescent Thermometer

Xingtang Rao,[†] Tao Song,[†] Junkuo Gao,[†] Yuanjing Cui,[†] Yu Yang,[†] Chuande Wu,[‡] Banglin Chen,*[,†,§] and Guodong Qian*[,†]

[†]State Key Laboratory of Silicon Materials, Cyrus Tang Center for Sensor Materials and Applications, Department of Materials Science & Engineering, Zhejiang University, Hangzhou 310027, China

[‡]Department of Chemistry, Zhejiang University, Hangzhou, 310027, China

[§]Department of Chemistry, University of Texas at San Antonio, San Antonio, Texas 78249, United States

Supporting Information

ABSTRACT: A new mixed lanthanide metal–organic framework thermometer $Tb_{0.9}Eu_{0.1}PIA$ with the significantly high sensitivity of 3.53% per K has been realized by making use of an organic ligand, 5-(pyridin-4-yl)isophthalate, with higher triplet state energy.

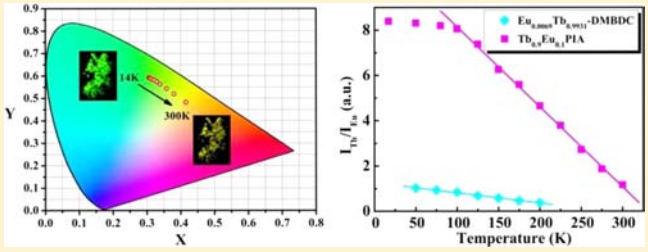

INTRODUCTION

Metal–organic frameworks (MOFs), self-assembled from metal ions or clusters with organic linkers, have been emerging as very promising multifunctional materials. Because the pores within such porous materials can be readily tuned while the functional sites can be straightforwardly immobilized into the pore surfaces for their specific recognitions of molecules, porous MOFs have wide applications in gas storage, separation, sensing, heterogeneous catalysis, and drug delivery.[1] Furthermore, because both inorganic metal ions or clusters and organic linkers can introduce magnetic, electronic, and luminescence properties through the deliberate selection of inorganic and organic building units, MOFs are also very promising platforms for these kinds of functional materials and devices.[1−14]

MOF thermometers have been only recently realized through the mixed-lanthanide metal–organic framework (M'LnMOF) approach.[15] Such luminescence-based thermometers have some unique and different features from conventional temperature sensors because of they are noninvasive and accurate, give fast response and high spatial resolution characteristics, and are able to work in even strong electromagnetic fields and fast-moving objects.[16−22]

The recently developed M'LnMOF methodology for luminescent thermometers is based on the energy transfer from the Tb^{3+} to Eu^{3+} ions within the framework solids.[15,19−22] As shown in Figure 1, organic ligands with suitable triplet state energy in the range of 22000 to 27000 cm^{-1} are the prerequisite to sensitize both Eu^{3+} and Tb^{3+} emissions.[2,3,23−25] Because the triplet state energy (T_1) of the organic ligands can tune the energy transition efficiency and kinetics of nonradiative transitions of $^5D_0$ to T_1 for the Eu^{3+} (k_1^{Eu}) and $^5D_4$ to T_1 for the Tb^{3+} (k_1^{Tb}), which accordingly affect the kinetics of

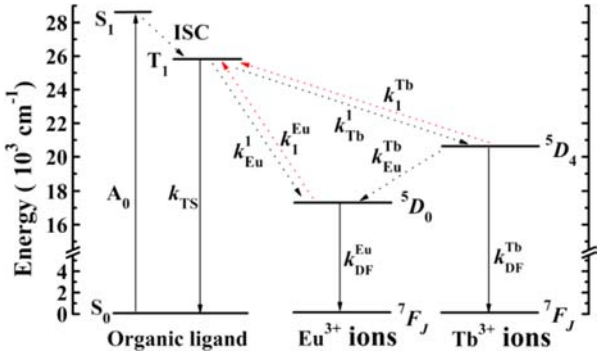

Figure 1. Schematic representation of energy absorption, migration, emission, and processes in luminescent mixed-lanthanide MOF thermometers. Abbreviations: S = singlet; T = triplet, A = absorption probability; ISC = intersystem crossing; k = radiative or nonradiative transition probability. The solid arrows represent singlet–singlet absorption and radiative transitions; dotted arrows indicate nonradiative transitions.

the radiative transitions of the $^5D_0 \rightarrow {}^7F_J$ transition of Eu^{3+} (k_{DF}^{Eu}) and of the $^5D_4 \rightarrow {}^7F_J$ transition of Tb^{3+} (k_{DF}^{Tb});[2,3,26] we, in principle, can modulate the temperature-dependent luminescence of the $^5D_0 \rightarrow {}^7F_2$ transition of Eu^{3+} at 615 nm and of the $^5D_4 \rightarrow {}^7F_5$ transition of Tb^{3+} at 546 nm by making use of different organic ligands of variable T_1 and thus optimize or maximize the sensitivity of the M'LnMOF luminescent thermometers.[22,26−28] The T_1 of DMBDC in our recently developed M'LnMOF thermometer $Eu_{0.0069}Tb_{0.9931}$-DMBDC

Received: July 19, 2013
Published: September 24, 2013

   dx.doi.org/10.1021/ja407219k | J. Am. Chem. Soc. 2013, 135, 15559−15564

(DMBDC = 2,5-dimethoxy-1,4-benzenedicarboxylate) is about 23306 cm^{-1},[15] which is not significantly higher than $^5D_0$ of the Eu^{3+} (17200 cm^{-1}) and $^5D_4$ of the Tb^{3+} (20500 cm^{-1}), leading to the comparable radiative transition kinetics of k_{DF}^{Eu} and k_{DF}^{Tb} and low sensitivity of this M'LnMOF thermometer.[29] We speculate that if we can incorporate an organic ligand of much higher T_1 into the M'LnMOFs to significantly differentiate the radiative transition kinetics of k_{DF}^{Eu} and k_{DF}^{Tb} (Scheme S1 in the Supporting Information) and thus to lead to the completely different temperature-dependent luminsecence of the $^5D_0 \rightarrow {}^7F_2$ transition of Eu^{3+} and the $^5D_4 \rightarrow {}^7F_5$ transition of Tb^{3+},[22] we should be able to target new M'LnMOF thermometers of much higher sensitivity. Herein we report a new M'LnMOF thermometer $Tb_{0.9}Eu_{0.1}PIA$ ($Tb_{0.9}Eu_{0.1}(PIA)(HPIA)(H_2O)_{2.5}$; H_2PIA = 5-(pyridin-4-yl)isophthalic acid) whose sensitivity is more than nine times higher than $Eu_{0.0069}Tb_{0.9931}$-DMBDC in an even broader temperature range of 100 to 300 K.

EXPERIMENTAL SECTION

Synthesis of $Ln(C_{13}H_7O_4N)(C_{13}H_8O_4N)(H_2O)_{2.5}$ (LnPIA). Taking TbPIA as an example, 5-(pyridin-4-yl)isophthalic acid (H_2PIA, 75.0 mg, 0.3 mmol), $Tb(NO_3)_3(H_2O)_6$ (140.0 mg, 0.3 mmol), and water (60 mL) were sealed into a 100 mL Teflon cup. After the resulting solution had been kept at 160 °C for 2 days, it was cooled to room temperature, and colorless rod-like crystals were collected by filtration and washed with DMF and H_2O (66.7 mg, 65% based on H_2PIA). Anal. Calcd for $Tb(C_{13}H_7O_4N)(C_{13}H_8O_4N)$ ($C_{26}H_{20}N_2O_{10.5}Tb$): C, 45.43; H, 2.93; N, 4.08. Found: C, 45.23; H, 2.81; N, 4.11. Other crystals were synthesized similarly to TbPIA except for the use of $Ln(NO_3)_3(H_2O)_6$.

Synthesis of $Tb_{1-x}Eu_x(C_{13}H_7O_4N)(C_{13}H_8O_4N)(H_2O)_{2.5}$ ($Tb_{1-x}Eu_xPIA$). The Tb/Eu mixed MOFs $Tb_{1-x}Eu_xPIA$ (x = 0.01, 0.05, 0.10, 0.20, 0.50, and 0.80) were synthesized similarly to TbPIA except for the use of a mixture of $Tb(NO_3)_3(H_2O)_6$ and $Eu(NO_3)_3(H_2O)_6$.

X-ray Crystallography. Single-crystal data were collected on Oxford Xcalibur Gemini Ultra diffractometer with an Atlas detector using graphite-monochromatic Mo Kα radiation (λ = 0.71073 Å) at 293 K. The determination of the unit cells and data collections for the crystal of TbPIA were performed with CrysAlisPro. The data sets were corrected by empirical absorption correction using spherical harmonics, implemented in SCALE3 ABSPACK scaling algorithm. The structure was solved by direct methods, and refined by full-matrix least-squares method with the SHELX-2013 program package. All non-hydrogen atoms including solvent molecules were located successfully from Fourier maps and were refined anisotropically. The H atoms on C atoms were generated geometrically. The H atoms of the aqua ligand are clearly visible in difference maps and were processed in the subsequent refinement with fixed isotropic displacement parameters. The H atoms on lattice water molecules are not located. CCDC 941416 contains the supplementary crystallographic data for this paper. These data can be obtained free of charge from The Cambridge Crystallographic Data Centre via www.ccdc.cam.ac.uk/data_request/cif.

Materials and Characterization. All the chemicals were commercially available and used without further purification. The 5-(pyridin-4-yl)isophthalic acid was synthesized according to the ref 30. Thermogravimetric analyses (TGA) were carried out on a Netzsch TG209F3 with a heating rate of 5 °C/min in N_2 atmosphere. Infrared spectrum (IR) was recorded on Thermo Fisher Nicolet iS10 spectrometer using KBr pallets. Elemental analyses for C, H, and N were performed on an EA1112 microelemental analyzer. Inductively coupled plasma spectroscopy (ICP) was performed on a Thermo XSENIES ICP-MS. The Tb/Eu ratios of $Tb_{1-x}Eu_xPIA$ were determined by ICP analysis (ICP samples were prepared by digesting the dry samples of $Tb_{1-x}Eu_xPIA$ into concentrated HCl (37%) followed by the dilution to 0.5% HCl solution). Comparison of the molar ratios of the starting Tb/Eu salts and those in $Tb_{1-x}Eu_xPIA$ products determined by ICP analysis are shown in Table S3, Supporting Information. Powder X-ray diffraction (PXRD) patterns were collected in the 2θ = 5–50° range on an X'Pert PRO diffractometer with Cu Kα (λ = 1.542 Å) radiation at room temperature. Luminescence spectra for the solid samples were recorded by a Hitachi F4600 fluorescence spectrometer. The photomultiplier tube voltage was 750 V and the scan speed was 240 nm/min, while the slit widths of excitation and emission spectra were 2.5 nm and 1.5 nm for H_2PIA, LnPIA (Ln = Y, Dy, Sm), and 1.0 and 1.0 nm for the other samples, respectively. The temperature-dependent emission spectra and the luminescence decay curve were recorded on an Edinburgh Instrument F920 spectrometer, both the excitation and emission slits are 1.0 nm, peak count is 5000, and the channel is 500. The overall quantum yields of the solid-state samples were determined by an absolute method using an integrating sphere (150 mm diameter, $BaSO_4$ coating) on an Edinburgh Instrument F920 spectrometer and acquired by the following formula [eq 1]

$$\Phi_{overall} = \frac{A_H}{R_{ST} - R_H} \quad (1)$$

where A_H is the area under emission spectrum of the sample and R_{ST} and R_H are diffuse reflectance of the reflecting standard and the sample, respectively. The estimated errors for quantum yields and luminescent lifetimes are within 5%.

RESULTS AND DISCUSSION

A series of isostructural lanthanide MOFs, $Ln(PIA)(HPIA)(H_2O)_{2.5}$ (LnPIA; Ln = Y^{3+}, Dy^{3+}, Sm^{3+}, Eu^{3+}, Tb^{3+}, Gd^{3+}; H_2PIA = 5-(pyridin-4-yl)isophthalic acid) were hydrothermally synthesized by the reaction of H_2PIA with $Ln(NO_3)_3$ at 160 °C for 2 days. The crystalline products once formed are insoluble in most common organic solvents. Taking TbPIA as an example, it crystallizes in the orthorhombic space group *Pba*2 (Table S1, Supporting Information) with two PIA ligands, one Tb atom, and 2.5 H_2O molecules in the asymmetric unit. The Tb atom is nine-coordinated with two O atoms from two water molecules and seven carboxylate oxygen atoms from four PIA ligands. The framework of TbPIA is composed of mononuclear $Tb(COO)_4$ secondary building units (Figure 2a) that are

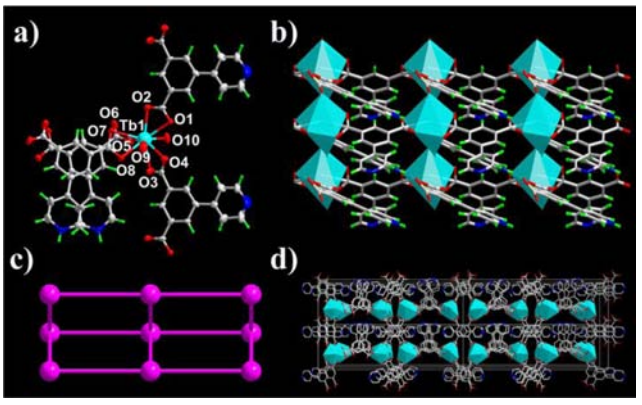

Figure 2. X-ray crystal structure of TbPIA showing (a) coordination environments around Tb^{3+}, (b) two-dimensional framework, (c) 2D (4, 4) square planar topology, and (d) 3D packing viewed along *b* axis.

bridged by the PIA ligands to form a two-dimensional layer framework (Figure 2b) of the (4, 4) square planar grid topology (Figure 2c). The 2D layers are packed together by weak intermolecular van der Waals interactions and aromatic $\pi-\pi$ interactions to form quite condensed 3D structure. All LnPIA MOFs are isostructural, as shown in their powder X-ray diffractions (Figure S2, Supporting Information).

dx.doi.org/10.1021/ja407219k | J. Am. Chem. Soc. 2013, 135, 15559–15564

The emission and excitation spectra measured at room temperature for the powder samples of H_2PIA ligand and LnPIA MOFs are displayed in Figure S5−S7, Supporting Information. The free H_2PIA ligand exhibits a weak emission at 408 nm, presumably due to $\pi \rightarrow \pi^*$ transitions under 330 nm UV light excitation (Figure S5a, Supporting Information). YPIA exhibits a red-shifted emission of the H_2PIA ligands at 482 nm with the excitation at 380 nm (Figure S5b, Supporting Information). Under 360 nm excitation, DyPIA exhibits both the red-shifted emission of the H_2PIA ligands at about 445 nm and the characteristic transitions ($^4F_{9/2} \rightarrow {}^6H_J$, J = 15/2, 13/2, 11/2) of Dy^{3+} at 482, 573, and 661 nm, respectively (Figure S6a, Supporting Information). Similarly, under 360 nm excitation, SmPIA exhibits both the red-shifted emission of the H_2PIA ligands at about 445 nm and the characteristic transitions ($^4G_{5/2} \rightarrow {}^6H_J$, J = 5/2, 7/2, 9/2) of Sm^{3+} at 561, 596, and 644 nm, respectively (Figure S6b, Supporting Information). With the excitation at 360 nm, TbPIA exhibits very strong characteristic transitions ($^5D_4 \rightarrow {}^7F_J$, J = 6−3) of Tb^{3+} at 491, 546, 585, and 622 nm, while EuPIA displays the characteristic transitions ($^5D_0 \rightarrow {}^7F_J$, J = 1−4) of Eu^{3+} at 594, 615, 650, and 699 nm (Figure S7, Supporting Information). The different luminescent behaviors of these lanthanide MOFs suggest that the intramolecular energy transfers from the PIA ligand to Tb^{3+} and Eu^{3+} are much more effective than those to Dy^{3+} and Sm^{3+}.[31]

Because these LnMOFs are isostructural, we can straightforwardly synthesize a series of M'LnMOFs in which different types of lanthanide ions of variable molar ratios can be systematically incorporated into the frameworks. The unique luminescent properties of Eu^{3+} and Tb^{3+} ions in their M'LnMOFs motivated us to dope small amounts of Eu^{3+} into the TbPIA framework to get $Tb_{1-x}Eu_x$PIA as the new M'LnMOF thermometers.

The temperature-dependent photoluminescent (PL) properties of these LnMOFs and M'LnMOFs were investigated both in terms of intensity and lifetime in order to establish their potentials as luminescent thermometers. The temperature-dependent emission spectra of TbPIA and EuPIA from 14 to 300 K are illustrated in Figure 3a,b, and the intensities and lifetimes of the $^5D_4 \rightarrow {}^7F_5$ (Tb^{3+}, 546 nm) and $^5D_0 \rightarrow {}^7F_2$ (Eu^{3+}, 615 nm) transitions are shown in Figure 3c,d. As expected, the emission intensity and lifetime of Tb^{3+} in TbPIA decrease gradually as the temperature increases, which is normally due to the thermal activation of nonradiative-decay pathways.[32−34] Although the nonradiative processes may lead to local heating, this type of heat is too small to influence the samples' temperature during the measurements, so such processes have no effect on the temperature-dependent luminescence. The emission intensity of Tb^{3+} decreases by 0.65% per K on increasing temperature from 225 to 300 K, while the decay lifetime decreases by 2.95 μs per K.

The luminescent behaviors of Tb^{3+} in TbPIA are comparable to those in Tb-DMBDC; however, those of Eu^{3+} in EuPIA are significantly different from the luminescent properties of Eu^{3+} in Eu-DMBDC: the emission intensity and lifetime of Eu^{3+} in EuPIA decreases much more slowly than those in Eu-DMBDC with the temperature increases.[15] This is because the expected energy difference of 8666 cm^{-1} between the excited triplet state of the ligand H_2PIA (25866 cm^{-1}) and the Eu^{3+} emitting level ($^5D_0$, 17200 cm^{-1}) in EuPIA is much larger than the difference of 6106 cm^{-1} in Eu-DMBDC to prohibit thermally driven depopulation.[20−22,35] Such significantly different luminescent

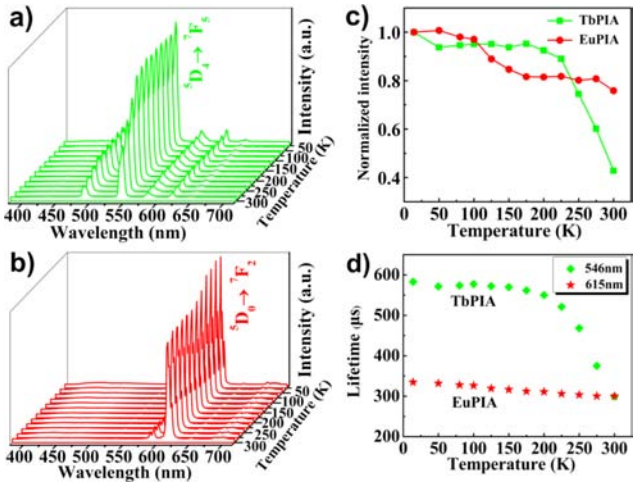

Figure 3. Emission spectra of (a) TbPIA and (b) EuPIA recorded between 14 and 300 K (excited at 360 nm, (c) temperature-dependent intensity of the $^5D_4 \rightarrow {}^7F_5$ transition of TbPIA and $^5D_0 \rightarrow {}^7F_2$ transition of EuPIA, and (d) temperature dependence of the $^5D_4$ lifetime for TbPIA and $^5D_0$ lifetime for EuPIA. The decay curves are monitored at 546 and 615 nm, respectively, and excited at 360 nm.

emissions of Tb^{3+} and Eu^{3+} in TbPIA and EuPIA should enable us to develop new luminescent mixed lanthanide $Tb_{1-x}Eu_x$PIA thermometers based on the temperature-dependent Tb^{3+}/Eu^{3+} emission intensity ratios of much higher sensitivity. To confirm our hypothesis, we synthesized the GdPIA to elucidate the triple energy levels of the ligand.[36,37] The low-temperature phosphorescence spectrum of the GdPIA under 335 nm excitation at 77 K was shown in Figure S10, Supporting Information. The estimated triplet energy level of the H_2PIA ligand from this study is 26455 cm^{-1}, which matches with the calculated one of 25866 cm^{-1} by DFT quite well.

As expected, the representative mixed lanthanide MOF $Tb_{0.9}Eu_{0.1}$PIA exhibits a significantly different temperature-dependent luminescent behavior (Figure 4) with respect to the emissions of Eu^{3+} at 615 nm and Tb^{3+} at 546 nm. With the temperature increases, the emission intensity of both Tb^{3+} and Eu^{3+} ions remain unchanged in the low temperature range (14−100 K). However, in the 100−300 K temperature range, the emission intensity of the Tb^{3+} ions decreases, while that of the Eu^{3+} increases. The absolute temperature measurement can be linearly correlated to an experimental parameter Δ ($\Delta = I_{Tb}/I_{Eu}$; I_{Tb} and I_{Eu} are the emission intensities of the $^5D_4 \rightarrow {}^7F_5$ (Tb^{3+} at 546 nm) and the $^5D_0 \rightarrow {}^7F_2$ (Eu^{3+} at 615 nm) transitions, respectively, at different temperature), by eq 2 from 100 to 300 K

$$\Delta = 11.671 - 0.0353T \quad (2)$$

This suggests that $Tb_{0.9}Eu_{0.1}$PIA is an excellent luminescent thermometer in this temperature range. As shown in Figure 4c, the sensitivity of this new M'LnMOF is about 9 times higher than that of our recently developed $Eu_{0.0069}Tb_{0.9931}$-DMBDC: 3.53% per K in $Tb_{0.9}Eu_{0.1}$PIA versus 0.38% per K in $Eu_{0.0069}Tb_{0.9931}$-DMBDC.[15] Such significantly enhanced sensitivity is really remarkable, which will allow us to highly sensitize the temperature changes. Furthermore, such M'LnMOF thermometer does not require any additional calibration of luminescence intensity and thus is much more instantaneous than other types of solid luminescent thermometers.[21,38,39] It worth noting that the sensitivity can be further enhanced by

dx.doi.org/10.1021/ja407219k | J. Am. Chem. Soc. 2013, 135, 15559−15564

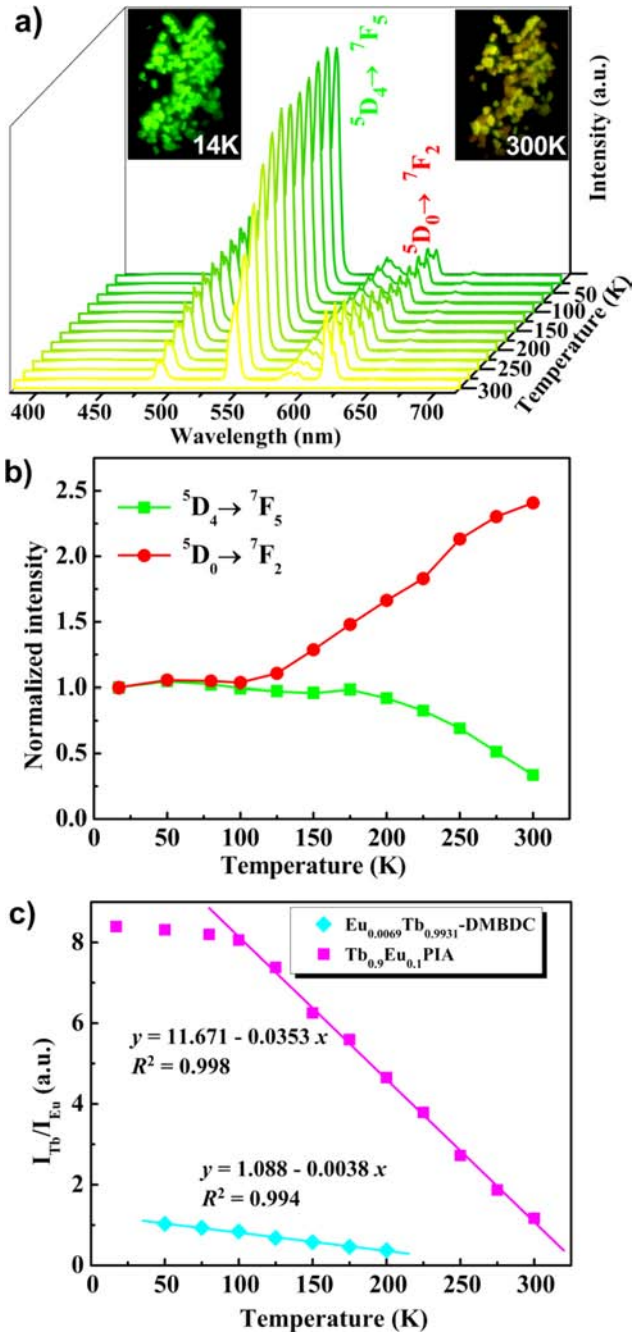

Figure 4. (a) Emission spectra of $Tb_{0.9}Eu_{0.1}$PIA recorded between 14 and 300 K (excited at 360 nm), (b) temperature-dependent intensity of the $^5D_4 \rightarrow {}^7F_5$ and $^5D_0 \rightarrow {}^7F_2$ transition for $Tb_{0.9}Eu_{0.1}$PIA, and (c) temperature-dependent intensity ratio of Tb^{3+} (546 nm) to Eu^{3+} (615 nm) and the fitted curve for $Tb_{0.9}Eu_{0.1}$PIA and $Eu_{0.0069}Tb_{0.9931}$-DMBDC. The insets of panel a are the optical photographs of luminescent $Tb_{0.9}Eu_{0.1}$PIA at 14 K (left) and 300 K (right) excited under 365 nm UV lamps.

increasing the Tb^{3+} content in the mixed LnMOFs. In fact, the sensitivity can be increased to be about 6% and 20% for the $Tb_{0.95}Eu_{0.05}$PIA and $Tb_{0.99}Eu_{0.01}$PIA luminescent thermometers (Figure S11 and S12, Supporting Information), respectively. Although $Tb_{0.99}Eu_{0.01}$PIA is not a reliable luminescent sensor because of the significantly low luminescent intensity from Eu^{3+} emission, the $Tb_{0.95}Eu_{0.05}$PIA with sensitivity of about 6% is also a potentially useful luminescent thermometer.

The temperature-dependent luminescence colors of $Tb_{0.9}Eu_{0.1}$PIA can be systematically tuned from green to yellow from 14 to 300 K, which can be clearly and directly observed even by the naked eye or camera (Figure 4a). Based on the Commission Internacionale d'Eclairage (CIE) chromaticity diagram, the corresponding CIE coordinates change from (0.3064, 0.5923) at 14 K to (0.4155, 0.4823) at 300 K (Figure S9, Supporting Information).

The robustness of the luminescent thermometer was demonstrated by the reversible luminescence under thermocycles. As shown in Figure S16, Supporting Information, the changes of the emission intensity radios of Tb^{3+} and Eu^{3+} ions (I_{Tb}/I_{Eu}) of $Tb_{0.9}Eu_{0.1}$PIA in the temperature range of 100 and 300 K are reversible. Furthermore, as showed in Figure S17, Supporting Information, the $Tb_{0.9}Eu_{0.1}$PIA samples from different batches exhibit basically same temperature-dependent luminescent spectra and display the same sensitivity of 3.53% per K.

The high temperature sensitivity of $Tb_{0.9}Eu_{0.1}$PIA is related to both different temperature-dependent emissions of Tb^{3+} and Eu^{3+} ions, and temperature-dependent energy transfer probability from the Tb^{3+} and Eu^{3+} ions. As shown in Figure 5a,

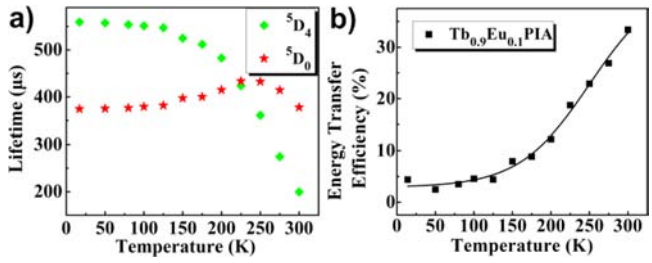

Figure 5. (a) Temperature dependence of the $^5D_4$ and $^5D_0$ lifetime (10–300 K) for $Tb_{0.9}Eu_{0.1}$PIA. The decay curves are monitored at 546 and 615 nm, respectively, and excited at 360 nm. (b) Temperature dependence of the energy transform efficiency from Tb^{3+} to Eu^{3+} ions in $Tb_{0.9}Eu_{0.1}$PIA.

$Tb_{0.9}Eu_{0.1}$PIA exhibits shorter $^5D_4$ (Tb^{3+}) lifetime than TbPIA but longer $^5D_0$ (Eu^{3+}) lifetime than EuPIA at the same temperature. Furthermore, the lifetime of $^5D_4$ in $Tb_{0.9}Eu_{0.1}$PIA decreases gradually as the temperature increases, while the lifetime of $^5D_0$ increases from 374.66 μs at 14 K to 433.83 μs at 225 K and then reduces to 378.0 1 μs at 300 K. These phenomena indicate that energy transfer from the Tb^{3+} to Eu^{3+} occurs. In theory, the efficiency of energy transfer (η_{ET}) from Tb^{3+} to Eu^{3+} ions may be estimated from eq 3,[40]

$$\eta_{ET} = \frac{\tau_1^{-1} - \tau_0^{-1}}{\tau_1^{-1}} \quad (3)$$

where τ_0 and τ_1 are luminescence lifetimes monitoring $^5D_4$ emission of Tb^{3+} ion at 546 nm of TbPIA and $Tb_{0.9}Eu_{0.1}$PIA, respectively. As shown in Figure 5b, between 14 and 125 K, the values of η_{ET} remain unchanged at a low temperatures. At the 125–300 K temperature range, the values of η_{ET} display stable enhancement at the elevated temperature, which might be mainly controlled by the phonon-assisted Förster transfer mechanism.[41,42]

CONCLUSION

In summary, we have targeted a new mixed lanthanide metal–organic framework thermometer $Tb_{0.9}Eu_{0.1}$PIA with the

dx.doi.org/10.1021/ja407219k | J. Am. Chem. Soc. 2013, 135, 15559–15564

significantly enhanced sensitivity of 3.53% per K by making use of an organic ligand 5-(pyridin-4-yl)isophthalate with higher triplet state energy. Because such M'LnMOF thermometers do not require any additional calibration of luminescence intensity, they are much more instantaneous than the widely explored luminescent solid thermometers. Luminescence-based thermometers are superior to other conventional thermometers because they can be noninvasive and accurate, provide fast response and high spatial resolution, and work in even strong electromagnetic fields and fast-moving objects.[43−46] These unique features together with the higher sensitivity and robustness of our $Tb_{0.9}Eu_{0.1}$PIA thermometer might enable it to be applied in practical applications. Furthermore, it also provides a new strategy to explore luminescence-based thermometers. Compared with those developed such as rare-earth doped materials, quantum dot clusters, organic dye molecules, gold−CdTe nanoparticles, and NIPAM based materials, which are pure inorganic or organic materials,[47−55] the M'LnMOF organic−inorganic hybrid materials as luminescent-based thermometers might have some advantages to tune their sensitivity more systematically by the implementation of a variety of organic linkers while still having compatibility with biological systems through the incorporation of specific organic moieties into the frameworks. We are now working on nanoscale M'LnMOF thermometers for instant and highly sensitive intracellular sensing and thermal mapping in biological systems in the near future.

■ ASSOCIATED CONTENT

Ⓢ Supporting Information

X-ray structure data in CIF format and characterization data. This material is available free of charge via the Internet at http://pubs.acs.org.

■ AUTHOR INFORMATION

Corresponding Authors

gdqian@zju.edu.cn
banglin.chen@utsa.edu

Notes

The authors declare no competing financial interest.

■ ACKNOWLEDGMENTS

This work was supported by the National Natural Science Foundation of China (Grant Numbers 51010002, 51272229, 51272231, and 51229201) and the Fundamental Research Funds for the Central Universities and partially supported by the Award AX-1730 from Welch Foundation (B.C.).

■ REFERENCES

(1) Zhou, H.-C; Long, J. R; Yaghi, O. M. *Chem. Rev.* **2012**, *112*, 673−1268.
(2) Binnemans, K. *Chem. Rev.* **2009**, *109*, 4283−4374.
(3) Cui, Y.; Yue, Y.; Qian, G.; Chen, B. *Chem. Rev.* **2012**, *112*, 1126−1162.
(4) White, K. A.; Chengelis, D. A.; Gogick, K. A.; Stehman, J.; Rosi, N. L.; Petoud, S. *J. Am. Chem. Soc.* **2009**, *131*, 18069−18071.
(5) Shustova, N. B.; McCarthy, B. D.; Dinca, M. *J. Am. Chem. Soc.* **2011**, *133*, 20126−20129.
(6) Qi, X. L.; Lin, R. B.; Chen, Q.; Lin, J. B.; Zhang, J. P.; Chen, X. M. *Chem. Sci.* **2011**, *2*, 2214−2218.
(7) Chandler, B. D.; Cramb, D. T.; Shimizu, G. K. H. *J. Am. Chem. Soc.* **2006**, *128*, 10403−10412.
(8) An, J.; Shade, C. M.; Chengelis-Czegan, D. A.; Petoud, S.; Rosi, N. L. *J. Am. Chem. Soc.* **2011**, *133*, 1220−1223.
(9) Stylianou, K. C.; Heck, R.; Chong, S. Y.; Bacsa, J.; Jones, J. T. A.; Khimyak, Y. Z.; Bradshaw, D.; Rosseinsky, M. J. *J. Am. Chem. Soc.* **2010**, *132*, 4119−4130.
(10) Rieter, W. J.; Taylor, K. M. L.; Lin, W. B. *J. Am. Chem. Soc.* **2007**, *129*, 9852−9853.
(11) Jiang, H. L.; Tatsu, Y.; Lu, Z. H.; Xu, Q. *J. Am. Chem. Soc.* **2010**, *132*, 5586−5587.
(12) Harbuzaru, B. V.; Corma, A.; Rey, F.; Atienzar, P.; Jordá, J. L.; García, H.; Ananias, D.; Carlos, L. D.; Rocha, J. *Angew. Chem., Int. Ed.* **2008**, *47*, 1080−1083.
(13) Takashima, Y.; Martínez, V. M.; Furukawa, S.; Kondo, M.; Shimomura, S.; Uehara, H.; Nakahama, M.; Sugimoto, K.; Kitagawa, S. *Nat. Commun.* **2011**, *2*, 168.
(14) Falcaro, P.; Furukawa, S. *Angew. Chem., Int. Ed.* **2012**, *51*, 8431−8433.
(15) Cui, Y.; Xu, H.; Yue, Y.; Guo, Z.; Yu, J.; Chen, Z.; Gao, J.; Yang, Y.; Qian, G.; Chen, B. *J. Am. Chem. Soc.* **2012**, *134*, 3979−3982.
(16) Sun, L. N.; Yu, J.; Peng, H.; Zhang, J. Z.; Shi, L. Y.; Wolfbeis, O. S. *J. Phys. Chem. C* **2010**, *114*, 12642−12648.
(17) Feng, J.; Tian, K.; Hu, D.; Wang, S.; Li, S.; Zeng, Y.; Li, Y.; Yang, G. *Angew. Chem., Int. Ed.* **2011**, *50*, 8072−8076.
(18) Jaque, D.; Vetrone, F. *Nanoscale* **2012**, *4*, 4301−4326.
(19) Miyata, K.; Konno, Y.; Nakanishi, T.; Kobayashi, A.; Kato, M.; Fushimi, K.; Hasegawa, Y. *Angew. Chem., Int. Ed.* **2013**, *52*, 1−5.
(20) Carlos, L. D.; Ferreira, R. A. S.; de Zea Bermudez, V.; Julian-Lopez, B.; Escribano, P. *Chem. Soc. Rev.* **2011**, *40*, 536−549.
(21) Brites, C. D. S.; Lima, P. P.; Silva, N. J. O.; Millan, A.; Amaral, V. S.; Palacio, F.; Carlos, L. D. *New J. Chem.* **2011**, *35*, 1177−1183.
(22) Brites, C. D. S.; Lima, P. P.; Silva, N. J. O.; Millan, A.; Amaral, V. S.; Palacio, F.; Carlos, L. D. *Adv. Mater.* **2010**, *22*, 4499−4504.
(23) Latva, M.; Takalo, H.; Mukkala, V. M.; Matachescu, C.; Rodríguez-Ubis, J. C.; Kankare, J. *J. Lumin.* **1997**, *75*, 149−169.
(24) Parker, D. *Coord. Chem. Rev.* **2000**, *205*, 109−130.
(25) Døssing, A. *Eur. J. Inorg. Chem.* **2005**, 1425−1434.
(26) Allendorf, M. D.; Bauer, C. A.; Bhakta, R. K.; Houk, R. J. T. *Chem. Soc. Rev.* **2009**, *38*, 1330−1352.
(27) Beeby, A.; Clarkson, I. M.; Dickins, R. S.; Faulkner, S.; Parker, D.; Royle, L.; de Sousa, A. S.; Williams, J. A. G.; Woods, M. *J. Chem. Soc., Perkin Trans. 2* **1999**, 493−503.
(28) Khalil, G. E.; Lau, K.; Phelan, G. D.; Carlson, B.; Gouterman, M.; Callis, J. B.; Dalton, L. R. *Rev. Sci. Instrum.* **2004**, *75*, 192−206.
(29) Carlos, L. D.; Ferreira, R. A.; Rainho, J. P.; de Zea Bermudez, V. *Adv. Funct. Mater.* **2002**, *12*, 819−823.
(30) Jia, J.; Athwal, H. S.; Blake, A. J.; Champness, N. R.; Hubberstey, P.; Schroder, M. *Dalton Trans.* **2011**, *40*, 12342−12349.
(31) Elbanowski, M.; Mąkowska, B. *J. Photochem. Photobiol. A: Chem.* **1996**, *99*, 85−92.
(32) Bhaumik, M. L. *J. Chem. Phys.* **1964**, *40*, 3711−3715.
(33) Weissman, S. I. *J. Chem. Phys.* **1942**, *10*, 214−217.
(34) Peng, H.; Stich, M. I. J.; Yu, J.; Sun, L. N.; Fischer, L. H.; Wolfbeis, O. S. *Adv. Mater.* **2010**, *22*, 716−719.
(35) Kolodner, P.; Tyson, J. A. *Appl. Phys. Lett.* **1983**, *42*, 117.
(36) Ramya, A. R.; Sharma, D.; Natarajan, S.; Reddy, M. L. P. *Inorg. Chem.* **2012**, *51*, 8818−8826.
(37) Xia, Z.; Wei, Q.; Yang, Q.; Qiao, C.; Chen, S.; Xie, G.; Zhang, G.; Zhou, C.; Gao, S. *CrystEngComm* **2013**, *15*, 86−99.
(38) Uchiyama, S.; de Silva, A. P.; Iwai, K. *J. Chem. Educ.* **2006**, *83*, 720−727.
(39) Feng, P. L.; Leong, K.; Allendorf, M. D. *Dalton Trans.* **2012**, *41*, 8869−8877.
(40) Rodrigues, M. O.; Dutra, J. D. L.; Nunes, L. A. O.; de Sá, G. F.; de Azevedo, W. M.; Silva, P.; Paz, F. A. A.; Freire, R. O.; Júnior, S. A. *J. Phys. Chem. C* **2012**, *116*, 19951−19957.
(41) Auzel, F. *Chem. Rev.* **2004**, *104*, 139−173.
(42) Liu, Y.; Qian, G.; Wang, Z.; Wang, M. *Appl. Phys. Lett.* **2005**, *86*, No. 071907.
(43) Wolfbeis, O. S. *Adv. Mater.* **2008**, *20*, 3759−3763.
(44) Haro-González, P.; Martínez-Maestro, L.; Martín, I. R.; García-Solé, J.; Jaque, D. *Small* **2012**, *8*, 2652−2658.

(45) Vetrone, F.; Naccache, R.; Zamarrón, A.; Juarranz de la Fuente, A.; Sanz-Rodríguez, F.; Martinez Maestro, L.; Martín Rodriguez, E.; Jaque, D.; García Solé, J.; Capobianco, J. A. *ACS Nano* **2010**, *4*, 3254−3258.
(46) Cauzzi, D.; Pattacini, R.; Delferro, M.; Dini, F.; Natale, C. D.; Paolesse, R.; Bonacchi, S.; Montalti, M.; Zaccheroni, N.; Calvaresi, M.; Zerbetto, F.; Prodi, L. *Angew. Chem., Int. Ed.* **2012**, *51*, 9662−9665.
(47) Sedlmeier, A.; Achatz, D. E.; Fischer, L. H.; Gorris, H. H.; Wolfbeis, O. S. *Nanoscale* **2012**, *4*, 7090−7096.
(48) Peng, H. S.; Huang, S. H.; Wolfbeis, O. S. *J. Nanopart. Res.* **2010**, *12*, 2729−2733.
(49) Biju, V.; Makita, Y.; Sonoda, A.; Yokoyama, H.; Baba, Y.; Ishikawa, M. *J. Phys. Chem. B* **2005**, *109*, 13899−13905.
(50) Chen, Y. Y.; Wood, A. W. *Bioelectromagnetics* **2009**, *30*, 583−590.
(51) Lee, J.; Govorov, A. O.; Kotov, A. N. *Angew. Chem., Int. Ed.* **2010**, *44*, 7439−7442.
(52) Chen, C. Y.; Chen, C. T. *Chem. Commun.* **2011**, *47*, 994−996.
(53) Wu, C.; Bull, B.; Szymanski, C.; Christensen, K.; McNeill, J. *ACS Nano* **2008**, *2*, 2415−2423.
(54) Wu, C.; Schneider, T.; Zeigler, M.; Yu, J.; Schiro, P. G.; Burnham, D. R.; McNeill, J. D.; Chiu, D. T. *J. Am. Chem. Soc.* **2010**, *132*, 15410−15417.
(55) Ye, F. M.; Wu, C. F.; Jin, Y. H.; Chan, Y. H.; Zhang, X. J.; Chiu, D. T. *J. Am. Chem. Soc.* **2011**, *133*, 8146−8149.